Vehicle Yaw Rate and Sideslip Estimations: A Comparative Analysis of SISO and MIMO Youla Controller Output Observer, Linear and Nonlinear Kalman Filters, and Kinematic Computation

Zhanzhan Liu[1] Francis Assadian[*2] Kevin Mallon[3]

Author Affiliations
1: Department of Mechanical & Aerospace Engineering, University of California Davis, California, United States
2: Department of Mechanical & Aerospace Engineering, University of California Davis, California, United States
3: Department of Mechanical & Aerospace Engineering, University of California Davis, California, United States

Correspondence
*fassadian@ucdavis.edu

Abstract

To reveal the benifits of a newly developed estimation technique Youla Controller Output Observer (YCOO) [1], this paper provides a comparative study of both SISO (Single Input Single Output) and MIMO (Multiple Input Multiple Output) YCOO and various types of Kalman Filters, such as (Linear) Kalman Filter (LKF), Extended Kalman Filter (EKF) and Unscented Kalman Filter (UKF), in estimating yaw rate and sideslip of a vehicle. We compare how each estimation technique performs and test the robustness of these estimators under plant parameters and environmental uncertainties, such as vehicle mass and tire-road coefficient of friction variations. We consider realistic situations such as sensor bias and provide analysis and potential solutions for YCOO when dealing with these practical problems. We will compare the yaw rate estimation result of these estimation approaches with a simple kinematic model methodology.

Keywords: Controller Output Observer, Kalman filter, Youla Parameterization, Yaw rate estimation, Sideslip Estimation

1 Introduction

Over the past years, there have been tremendous amounts of work in the vast area of dynamic system state and parameter estimation. Virtual sensing has become very popular as the cost of various sensors are continuously on the rise. The strategies used to devise state and parameter estimations include well-developed estimation techniques such as Kalman filtering [2], and nonlinear observers which present a robust estimator by a BMIs (Bilinear Matrix Inequality) and finding a convex solution to this estimator by posing the problem as an LMI (Linear Matrix Inequality) [3].

In almost all these studies, practical implementations of these estimators such as computation and calibration overheads are ignored. Most importantly, there has not been any investigation to illustrate the benefits, such as performance and robustness, of one technique over the other.

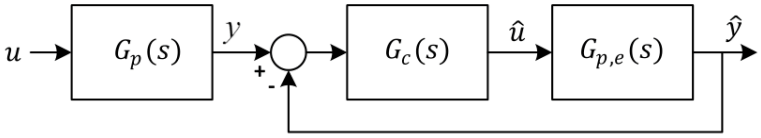

Figure 1 - General Controller Output Observer

In a previous study [1], we presented the newly developed Youla Controller Output Observer (YCOO), a deterministic estimation technique. The intent and contribution of this paper is to gain further insights into various estimation strategies by performing a comparative analysis of stochastic estimation techniques, different types of Kalman Filtering techniques, with YCOO in a popular vehicle dynamics application. The practical implications of these estimation strategies are that YCOO would require little to no calibration and computation overhead relative to other estimation approaches.

Two important points are noteworthy. The first is that YCOO, similar to stochastic filtering techniques, is applicable to both stable and unstable plants as discussed in [1], even though the plant under consideration in this paper is stable. The second point is all traditional estimation concepts require access to system input u. However, Controller Output Observer, COO, and YCOO does not have this constraint, as shown in Figure 1 and Figure 2 (where $G_p(s)$ represents the actual plant, while $G_{p,e}$ represents the plant model used for the estimation purposes). In fact, if the input is not known, an estimation of the unknown input can be obtained from YCOO.

The rest of this paper is organized as follows, in the remaining part of the introduction, we will briefly discuss vehicle yaw rate and sideslip estimation, YCOO, and Kalman filtering. In section 2, we discuss vehicle modeling including dealing with uncertainties. In section 3, state estimation for the SISO case including the simulation results are discussed, In section 4, we present the MIMO case, and finally in section 5, the conclusion and future work are presented.

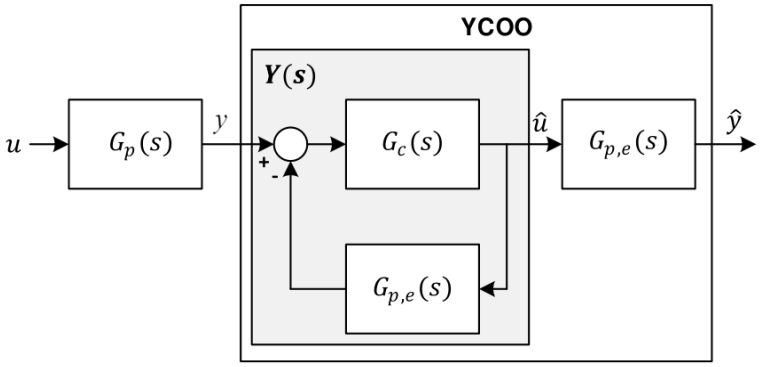

Figure 2 - Youla Controller Output Observer

1.1 Yaw Rate and Sideslip Estimation

As done in this paper, accelerometers can be implemented on-board vehicle for measuring lateral accelerations at particular locations of a vehicle so that good estimations of yaw rate and sideslip are obtained. Good estimations of yaw rate and sideslip by merely using accelerometers results in a significant reduction of vehicle stability control software implementation cost. Furthermore, sideslip estimation results in a better control of vehicle stability and hence, increase in vehicle safety. Equivalently, yaw rate estimation could be utilized for sensor diagnostic if the intent is not to replace the rate gyros.

When a car turns a corner, it exhibits a yaw rate and a lateral velocity in the direction perpendicular to the its orientation. If we use the center of gravity (c.g.) as a reference point, the direction that the body of the vehicle is pointing (true heading) is different from the direction that the vehicle is travelling (known as heading over ground) and the angle between these directions is called the vehicle sideslip angle [4]. Sideslip can be measured by optical correlation sensors which are extremely expensive. With a known sideslip angle, we can have a better understanding of the vehicle stability during a turn, and hence, improve its controllability and safety during stability maneuvers [4].

1.2 Youla Controller Output Observer (YCOO)

In [1], the authors utilize the Youla Parameterization (YCOO) approach for the purpose of estimator design. In this paper, as discussed earlier, we will use the same approach for the proposed comparative investigation. This methodology transforms state estimation to feedback control design, such as by designing a proper and stable controller G_c (derived by using Youla Parameterization approach), *COO*, as shown in Figure 1, the output of the feedback loop is forced to follow its reference target, which in this case, this target is precisely the measured sensor signal. By forcing the output of the feedback loop to follow its target, we are indirectly forcing our model, which is used for state estimation, to follow the actual plant. In this case, measured lateral acceleration including sensor noise, n, is used as a reference target, while the estimated lateral acceleration from our model (state space representation) is used as a feedback signal.

1.3 Kalman Filters

Kalman Filtering (LKF) is an estimation technique which uses a statistical approach to estimate the mean and co-variance of the states, by utilizing a plant model and sensor measurements, to find the best estimate of the actual states. However, since LKF uses a linear state space representation as a model, there are some limitations in the applications where plants are highly nonlinear, or sensor measurements are of poor qualities. For these applications, there are other types of Kalman Filters, such as the Extended Kalman Filter (EKF) and Unscented Kalman Filter (UKF).

To utilize the EKF, one must linearize the nonlinear system equations at each time step and utilizes the Jacobian matrices to estimate the variance matrix. This technique is widely used in state as well as certain parameter estimation. However, since the Jacobian matrices are required to be computed at each time step, the computational overhead can be high especially for systems with a large number of states. Furthermore, under certain circumstances, the stability and convergence of this approach cannot be guaranteed. The UKF uses the unscented transformation to sample the statistics associated with the plant model and sensor uncertainties to represent the mean and the co-variance at each time step without any need for linearization. Therefore, the UKF requires similar computational overhead relative to the EKF but it has shown better accuracy and convergence [5] and similar to EKF, it is also widely applied.

2 System Modeling

2.1 Vehicle Model

2.1.1 Nonlinear Bicycle Model with Pacejka Tire Model

One way to estimate the yaw rate is to use the lateral acceleration measurement at the vehicle center of gravity (c.g.) and the dynamic relationship between the yaw rate and lateral acceleration in steady state cornering. For a front steering vehicle, the system diagram of a simple vehicle dynamic model, using a two degrees of freedom bicycle model, is shown in Figure 3. Where U is the forward velocity, which is assumed to be constant. Parameters m and J are vehicle mass and moment of inertia. The distances between from the vehicle c.g. to the front and rear axles are respectively shown as a and b. The front and rear tire lateral forces are indicated by F_f and F_r respectively. The front wheel steering angle input δ, as illustrated. The model states are the lateral velocity V, and the yaw rate ω.

With body fixed coordinates, the equations of motion of the bicycle model are written as,

$$\dot{V} = \frac{F_f \cos\delta + F_r}{m} - U\omega \tag{1}$$

$$\dot{\omega} = \frac{F_f \cos\delta \cdot a + F_r \cdot b}{J} \tag{2}$$

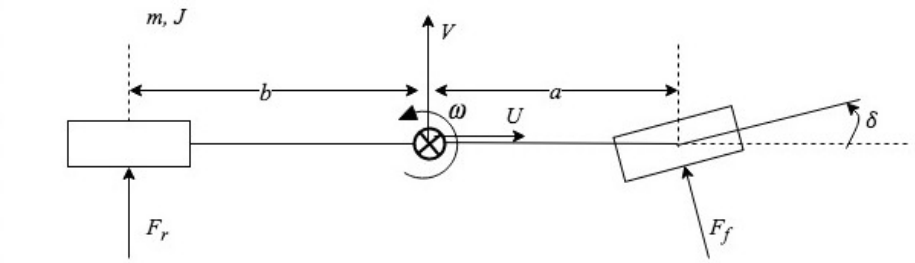

Figure 3 - Steering Bicycle Model System Diagram

The lateral forces exerted on the front and rear tires, F_f, F_r, are functions of the slip angles of the front and rear tires. The slip angles of the front and rear are related to the system input and the states as given below,

$$\alpha_f = \delta - \tan^{-1}\left(\frac{V + a\omega}{U}\right) \tag{3}$$

$$\alpha_f = \tan^{-1}\left(\frac{b\omega - V}{U}\right) \tag{4}$$

The lateral tire forces are functions of the tire slip angles and their relationship has been studied for many decades for developing an appropriate mathematical tire model. There are many tire models which relate the tire slip angles to the lateral tire forces. One commonly used and popular model is the Pacejka tire model, also known as the "Magic Formula" tire model. From [6], the basic formulas for lateral forces are,

$$F_f = D_f \cdot \sin\left(C \cdot \tan^{-1}\left(B_f\left((1-E)\alpha_f + \frac{E}{B_f}\cdot \tan^{-1}\left(B_f\alpha_f\right)\right)\right)\right) \tag{5}$$

$$F_r = D_r \cdot \sin\left(C \cdot \tan^{-1}\left(B_r\left((1-E)\alpha_r + \frac{E}{B_r}\cdot \tan^{-1}\left(B_r\alpha_r\right)\right)\right)\right) \tag{6}$$

where B, C, D and E are various tire parameters, such as B is the stiffness factor, C is the shape factor, D is the peak factor which is related to the tire normal force (F_z) and tire-road friction coefficient (μ_H), and E is the curvature factor. These coefficients are extracted from various tire testing and measurement data. We have utilized typical tire data in this paper.

Given a steering angle input and system state initial conditions, tire slip angles are computed from equations (3) and (4). Knowing the tire slip angles, tire forces are computed from equations (5) and (6). Having the tire forces, the equations of motion, (1) and (2), are solved for the solutions of the new states. This cycle is then repeated at each time step.

The lateral acceleration at c.g. is related to the front and rear tire forces and is given by,

$$a_y = \frac{F_f \cos\delta + F_r}{m} \tag{7}$$

This SISO model then consists of one input, the front road wheel angle, δ, and one output, the vehicle lateral acceleration at the c.g., a_y.

2.2 Kinematic Relationship

The lateral acceleration is kinematically related to the states V and ω as discussed below, and therefore, by measuring the lateral acceleration, an estimate of the yaw rate can be obtained. Given the distances between the c.g. and the axles, by measuring the lateral accelerations at the front and rear axles, we can kinematically estimate the yaw rate. As shown in Figure 4, the lateral accelerations a_f and a_r, with distances of S_1 and S_2 to the c.g., can be related to the states V and ω,

$$a_f = \dot{V} + U\omega - S_2\dot{\omega} \tag{8}$$

$$a_r = \dot{V} + U\omega + S_1\dot{\omega} \tag{9}$$

By rearranging equations (8) and (9), yaw rate can be derived from a_f and a_r,

$$\omega = \int \frac{a_f - a_r}{S_1 + S_2}\mathrm{d}t \tag{10}$$

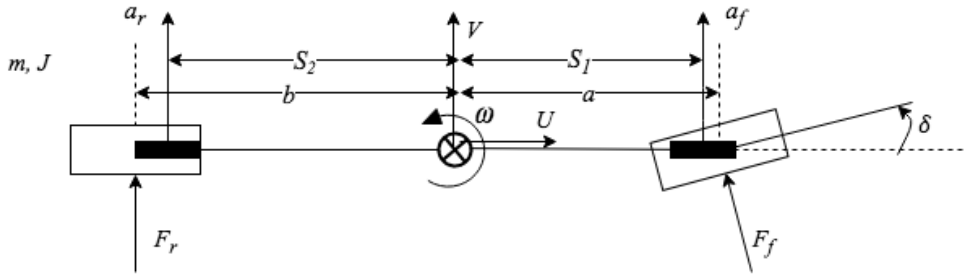

Figure 4 - Front Steering Bicycle Car Model System Diagram with two accelerometers.

Deriving the yaw rate using this kinematic relationship is one approach to estimate the yaw rate and this approach will be compared to the other estimation techniques discussed in this paper.

2.3 MIMO model

By adding another input, such as controlling the rear road wheel angle, and by measuring both front and rear axle lateral accelerations, we can transform the vehicle model from SISO to MIMO as shown in Figure 5. With one more input, the state equations (1) and (2) can be written as,

$$\dot{V} = \frac{F_f \cos\delta_f + F_r \cos\delta_r}{m} - U\omega \tag{11}$$

$$\dot{\omega} = \frac{aF_f \cos\delta - bF_r \cos\delta_r}{J} \tag{12}$$

The equations (3) and (4) are re-written as,

$$\alpha_f = \delta_f - \tan^{-1}\left(\frac{V + a\omega}{U}\right) \tag{13}$$

$$\alpha_f = \delta_r - \tan^{-1}\left(\frac{V - b\omega}{U}\right) \tag{14}$$

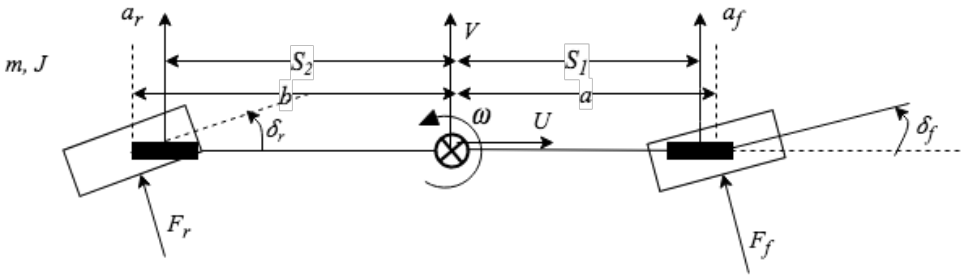

Figure 5 - Front and Rear Steering Bicycle Car Model System Diagram with two accelerometers.

The vehicle sideslip (β) is the angle between the actual direction of vehicle and the direction of longitudinal velocity. Since the magnitude of sideslip angle is normally not greater than 2^o [6], we can use the small angle approximation and it can be expressed as the ratio of the lateral velocity (V) and the longitudinal velocity (U),

$$\beta = \frac{V}{U} \tag{15}$$

Since we assume the longitudinal velocity, U, to be constant, instead of using the lateral velocity, V, we can use the vehicle sideslip β as one of the states. In this way, our state estimation will consist of estimating the vehicle sideslip and the yaw rate. Then using equations (15) and (11), we can write,

$$\dot{\beta} = \frac{F_f \cos\delta_f + F_r \cos\delta_r}{mU} - \omega \tag{16}$$

Then by substituting β in place of V into equations (13) and (14), the front and rear tire slip angles can be expressed as,

$$\alpha_f = \delta_f - \tan^{-1}\left(\beta + \frac{a\omega}{U}\right) \tag{17}$$

$$\alpha_f = \delta_r - \tan^{-1}\left(\beta - \frac{b\omega}{U}\right) \tag{18}$$

Then the lateral forces will be computed exactly the same as the SISO case.

The front and rear lateral accelerations can be related to the new state β by modifying equations (8) and (9) as follows,

$$a_f = U\dot{\beta} + U\omega - S_2\dot{\omega} \tag{19}$$

$$a_r = U\dot{\beta} + U\omega + S_1\dot{\omega} \tag{20}$$

This MIMO model then consists of two inputs, the front and rear road wheel angles, δ_f and δ_r, and two outputs, the vehicle lateral accelerations at the front and rear axles, a_f and a_r.

2.3.1 Linearizing the Bicycle Model for SISO and MIMO Cases

For the purpose of state estimations, both YCOO and LKF require a linearized model of the plant. Therefore, we need to linearize the vehicle and tire models to obtain a state space representation of the nonlinear plant to be used for YCOO and LKF estimators. For linearizing a bicycle model, all angles were assumed to be small, and equations (1) and (2) are re-written as,

$$\dot{V} = \frac{F_f + F_r}{m} - U\omega \tag{21}$$

$$\dot{\omega} = \frac{F_f \cdot a + F_r \cdot b}{J} \tag{22}$$

For linearizing a tire model, it is assumed that the lateral tire forces are proportional to slip angles with front and rear cornering stiffness coefficients C_f and C_r,

$$F_f = C_f \alpha_f \tag{23}$$

$$F_r = C_r \alpha_r \tag{24}$$

Then the state-space representation of the equations of motion for the SISO case is written as,

$$\begin{pmatrix} \dot{V} \\ \dot{\omega} \end{pmatrix} = \begin{pmatrix} -\frac{C_f + C_r}{mU} & -\left(\frac{aC_f - bC_r}{mU} + U\right) \\ -\frac{aC_f - bC_r}{JU} & -\frac{a^2C_f + b^2C_r}{JU} \end{pmatrix} \begin{pmatrix} V \\ \omega \end{pmatrix} + \begin{pmatrix} \frac{C_f}{m} \\ \frac{aC_f}{J} \end{pmatrix} \delta \tag{25}$$

The lateral acceleration at c.g a_y can be expressed as,

$$a_y = \begin{pmatrix} -\frac{C_f + C_r}{mU} & \frac{aC_f - bC_r}{mU} \end{pmatrix} \begin{pmatrix} V \\ \omega \end{pmatrix} + \begin{pmatrix} \frac{C_f}{m} \end{pmatrix} \delta \tag{26}$$

Similarly, knowing that the states for the MIMO case are the vehicle sideslip β and yaw rate ω, the state-space representation for this case can be expressed as,

$$\begin{pmatrix} \dot{\beta} \\ \dot{\omega} \end{pmatrix} = \begin{pmatrix} -\frac{C_f + C_r}{mU} & -\left(\frac{aC_f - bC_r}{mU^2} + 1\right) \\ -\frac{aC_f - bC_r}{J} & -\frac{a^2C_f + b^2C_r}{JU} \end{pmatrix} \begin{pmatrix} \beta \\ \omega \end{pmatrix} + \begin{pmatrix} \frac{C_f}{mU} & \frac{C_r}{mU} \\ \frac{aC_f}{J} & -\frac{br}{J} \end{pmatrix} \begin{pmatrix} \delta_f \\ \delta_r \end{pmatrix} \tag{27}$$

$$\begin{pmatrix} a_f \\ a_r \end{pmatrix} = \begin{pmatrix} -\frac{C_f + C_r}{m} - S_1 \frac{aC_f - bC_r}{J} & -\frac{aC_f - bC_r}{mU} - S_1 \frac{a^2C_f + b^2C_r}{JU} \\ -\frac{C_f + C_r}{m} + S_2 \frac{aC_f - bC_r}{J} & -\frac{aC_f - bC_r}{mU} + S_1 \frac{a^2C_f + b^2C_r}{JU} \end{pmatrix} \begin{pmatrix} \beta \\ \omega \end{pmatrix} + \begin{pmatrix} \frac{C_f}{m} + S_1 \frac{aC_f}{J} & \frac{C_r}{m} - S_1 \frac{bC_r}{J} \\ \frac{C_f}{m} - S_2 \frac{aC_f}{J} & \frac{C_r}{m} + S_2 \frac{bC_r}{J} \end{pmatrix} \begin{pmatrix} \delta_f \\ \delta_r \end{pmatrix} \quad (28)$$

These models are utilized to estimate the vehicle yaw rate for the SISO case, and the vehicle yaw rate and sideslip angle for the MIMO case.

2.4 Uncertainties

The acceleration sensor measurements in the simulation environment are made from a nonlinear model, a representation of the actual vehicle. While the YCOO and LKF utilize a linear model to estimate the states of this nonlinear plant. Therefore, for these estimators, model uncertainties include the differences between linear and nonlinear models used for state estimation and acceleration measurements respectively. In addition to this inherent uncertainty, we will examine parameter and environmental uncertainties, such as mass and tire-road coefficient of friction variations, for all estimator approaches discussed below, in the robustness test section of this paper.

For simulating sensor noise, data sheet of a single axis accelerometer SCA830-D05 [7] is utilized. From the data sheet, we can assume that the sensor noise has a zero mean and a variance of $R = 2.5 \times 10^{-3}$.

3 State Estimation, The SISO Case

In the state estimation for the SISO case, the linear model includes a front wheel steering vehicle with one accelerometer at the center of gravity of the vehicle for lateral acceleration measurement as shown in Figure 3. The input, in this case, is the front wheel steering angle (δ), and the output is the lateral acceleration at c.g (a_y). This model is utilized to estimate the vehicle yaw rate.

3.1 Youla Parameterization Control Design

The transfer function of the plant is the ratio between lateral acceleration and the road wheel angle,

$$G_p(s) = \frac{a_y}{\delta}(s) \quad (29)$$

The model of the plant is stable with no unstable/non-minimum phase zeros, which makes the controller design by the Youla parmeterization a straightforward case. Based on the Youla parameterization technique in [1], the Youla parameter can be computed by,

$$Y(s) = \frac{1}{G_p} T \tag{30}$$

where T is the desired closed-loop transfer function, and we select this desired transfer function to be a second order well damped filter with two additional poles at s = $1/\tau$ for better shaping of the Youla parameter at high frequency,

$$T(s) = \frac{\omega_n^2}{(s^2 + 2\zeta\omega_n s + \omega_n^2)(\tau s + 1)} \tag{31}$$

Then the Youla parameter is simply written as

$$Y(s) = \frac{1}{G_p} \cdot \frac{\omega_n^2}{(s^2 + 2\zeta\omega_n s + \omega_n^2)(\tau s + 1)} \tag{32}$$

The sensitivity transfer-function S of the feedback loop can be derived using the algebraic constraint between this transfer function and the closed-loop transfer function, T,

$$S(s) = 1 - T(s) \tag{33}$$

and finally, the controller G_c, to be used for the yaw rate estimation, can be calculated by,

$$G_c(s) = Y/S \tag{34}$$

With proper choice of ζ and ω_n, the controller, G_c, is designed so that the closed loop transfer function, T, is at 0 dB at low frequency which indicates good target following, and the sensitivity transfer function, S, is small in this frequency range which indicates good disturbance rejection. In selecting a bandwidth for the closed loop transfer function, T, a tradeoff between the transient response speed and the overshoot should be made. Figure 6 shows the bode plot of the plant model used in YCOO. The model has a high gain of 40 dB in the lower frequency region and this gain decreases starting around 1 rad/s and reaches the minimum at 20 dB around 6 rad/sec. If the bandwidth of the controller/estimator is designed to be greater than 1 rad/sec, then the controller gain will be higher in the frequency range where the model gain is lower (above 1 rad/sec). This may result in a poor transient behavior of the closed loop system due to a bigger overshoot.

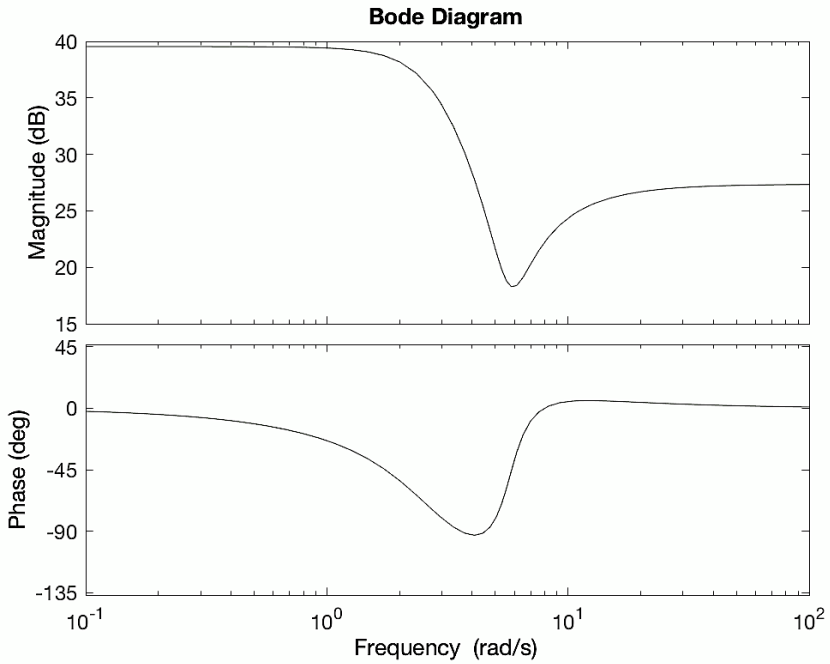

Figure 6 - Bode plot of linear plant.

As shown in Figure 7, T is at 0 dB for a wide range of frequencies. The estimation results of the Yaw rate and lateral acceleration are shown in Figure 8 and Figure 9. Both the yaw rate and the lateral acceleration estimations have excellent steady state target following. However, for the case of yaw rate, due to designing a closed loop with large bandwidth, there is a large overshoot during the transient response. This overshoot can only be reduced or eliminated by reducing the closed loop bandwidth. We have designed a new controller with reduced closed loop bandwidth and the results are presented in Figure 10, Figure 11, and Figure 12 . The Bode plots of T, S, and Y with a reduced bandwidth are shown in Figure 10.

The yaw rate estimation in Figure 11 shows drastic reduction in overshoot and oscillations during the transient. However, rise time, in this case, has been slightly increased. We have designed a final controller and further reduced the closed loop bandwidth as shown in Figure 13, Figure 14, and Figure 15. In this case, we can observe that the yaw rate overshoot and oscillations have been totally vanished, but this time, both rise time and settling time have been drastically increased. Steady state estimations have excellent target following for all these cases.

Regarding the bandwidth requirement/constraint, a set of objective requirements for the estimation results should be decided to reduce the subjectivity of our findings. For our comparative analysis in this paper, we will use the results of the YCOO with the highest bandwidth.

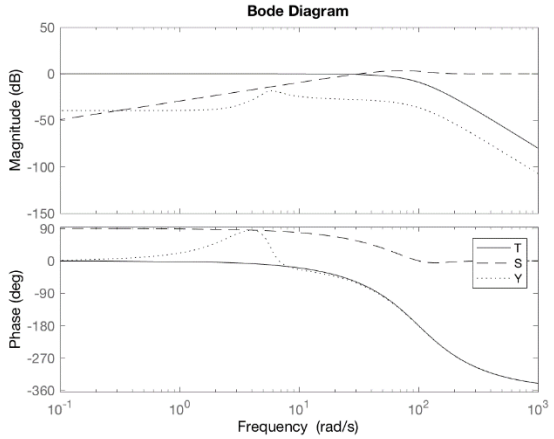

Figure 7 - Bode plot for SISO case with large bandwidth.

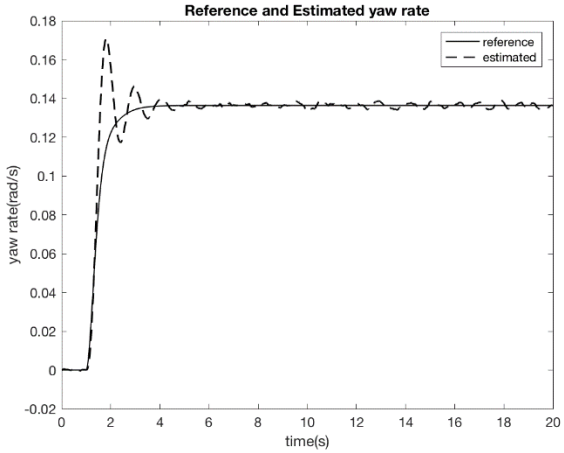

Figure 8 - Yaw rate estimation using YCOO with faster controller.

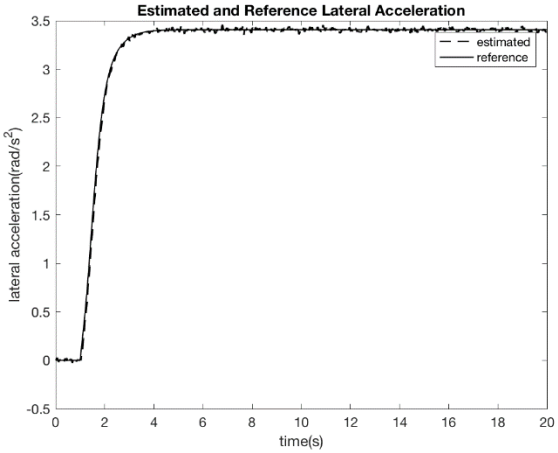

Figure 9 - Lateral acceleration estimation using YCOO with faster controller.

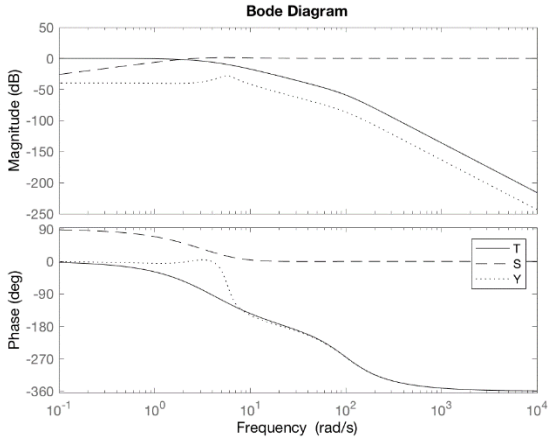

Figure 10 - Bode plot for SISO case with smaller bandwidth.

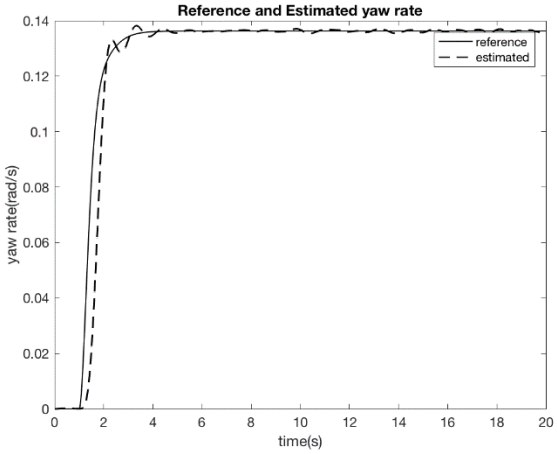

Figure 11 - Yaw rate estimation using YCOO with slower controller.

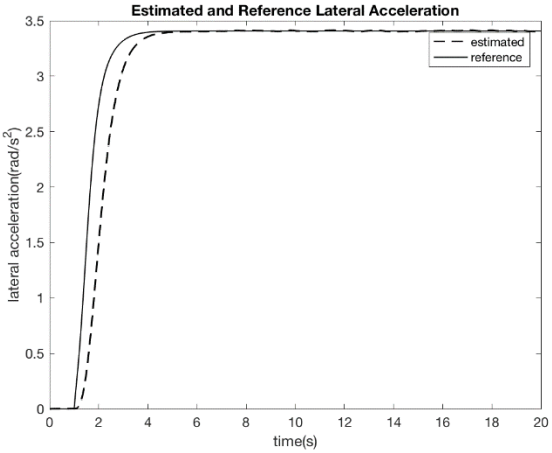

Figure 12 - Lateral acceleration estimation using YCOO with slower controller.

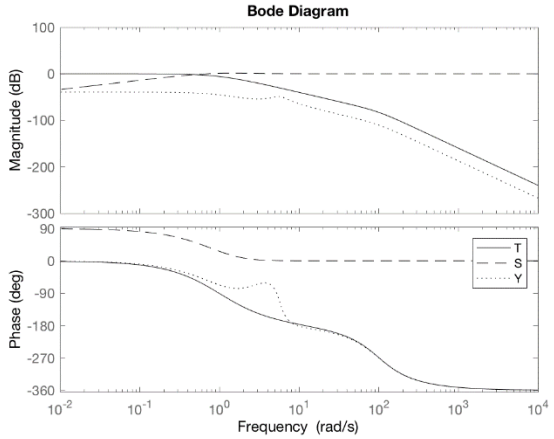

Figure 13 - Bode plot for SISO case with smallest bandwidth.

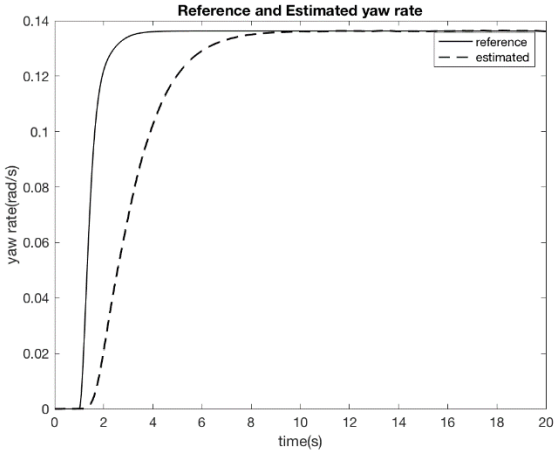

Figure 14 - Yaw rate estimation using YCOO with slowest controller.

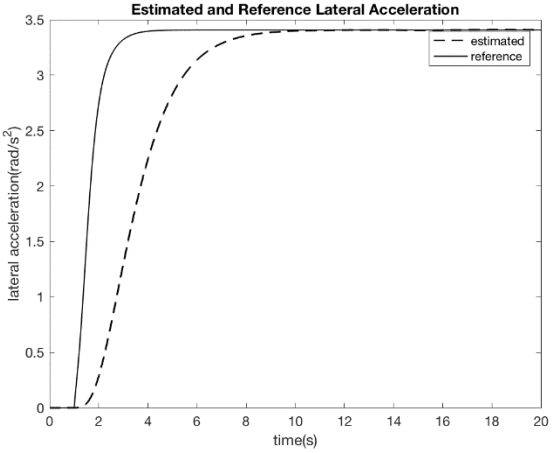

Figure 15 - Lateral acceleration estimation using YCOO with slowest controller.

To better understand the yaw rate overshoot problem, it is worthwhile to compute the closed loop transfer function from the yaw rate to road wheel angle T_ω using the previously designed G_c

and obtain its bode plot. The plant, $G_{p,\omega}$, transfer function from the yaw rate ω to the wheel angle input δ can be written as,

$$G_{p,\omega} = \frac{\omega}{\delta}(s) = \frac{\frac{aC_f}{J}s + \frac{(a+b)C_fC_r}{mJU}}{s^2 + \left(\frac{C_f + C_r}{mU} + \frac{a^2C_f + b^2C_r}{JU}\right)s + \left(\frac{(a+b)^2C_fC_r}{mJU^2} + \frac{bC_r - aC_f}{J}\right)} \quad (35)$$

Using the designed controller transfer function G_c, we can obtain the closed loop transfer function by,

$$T_\omega = \frac{G_cG_{p,\omega}}{1 + G_cG_{p,\omega}} \quad (36)$$

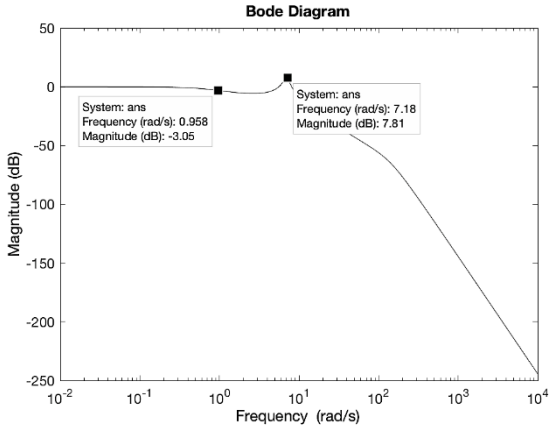

Figure 16 - Bode plot of closed loop transfer function of yaw rate estimation.

We can now obtain the bode plot of T_ω, as illustrated in Figure 16. By observing this bode plot, the gain of T_ω is at 0 dB at low frequency, and after 1 rad/s, the gain starts to decrease and then increase again around 7 rad/s and peak at around 10 rad/s. By tuning ζ and ω_n in the closed loop transfer function T, we can only modify the frequency of where the maximum gain in this bode plot is located. It is obvious that any closed loop bandwidth of T_ω greater than 1 rad/s does not result in good target following. If we decrease the bandwidth of T to 1 rad/s or even smaller, we indirectly decrease the bandwidth of T_ω and therefore, the yaw rate estimation will have a good target following behavior with no overshoot, but this obviously will slow down the estimation as shown in Figure 14.

3.2 Simulation Results

Figure 17 and Figure 18 show a comparison of the lateral acceleration at the c.g. and the yaw rate estimations using YCOO, LKF, EKF, and UKF with 2^o road wheel angle step input. For both the lateral acceleration and yaw rate estimates, all these strategies perform well in both areas of sensor noise attenuation and good target following. Figure 19 and Figure 20illustrate the results of the yaw rate estimations with 6^o and 10^o road wheel angle step input. As we increase the input, we can observe that LKF will have a steady state error as the vehicle model (tire forces) starts operating in the nonlinear region.

It should be noted that the lateral tire forces are linear at small tire slip angles and as the slip angle increases, the tire forces begin to operate in the nonlinear region and eventually at the very high tire slip angles, the lateral tire forces will saturate. As the tire slip angles increase, purely linear tire models will provide larger lateral forces than their nonlinear counterpart, and as a result, LKF overestimates the yaw rate.

It is interesting to observe that in the case of YCOO, although this strategy utilizes a linear tire and vehicle models, its robustness characteristics results in excellent steady state target following. The robustness characteristics of YCOO will be further investigated in the next section. However, as discussed in the last section, the closed loop bandwidth of YCOO is selected in such a way that its transient response due to the overshoot is not as good as the other techniques. The EKF and UKF perform well in both these cases as they are utilizing the same nonlinear vehicle model used for the reference generator. We will investigate the performance of the EKF and UKF in the robustness test of the next section when the model used for estimation differs from its nominal values.

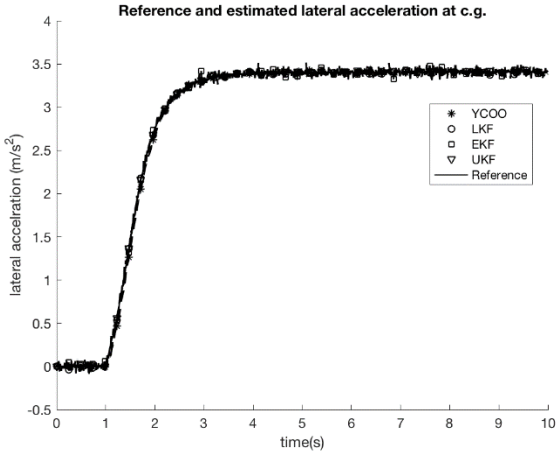

Figure 17 - Lateral acceleration estimation using different strategies with 2° road wheel angle step input

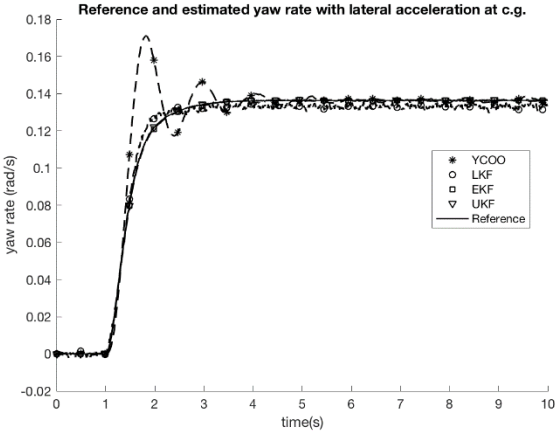

Figure 18 - Yaw rate estimation using different strategies with 2° road wheel angle step input.

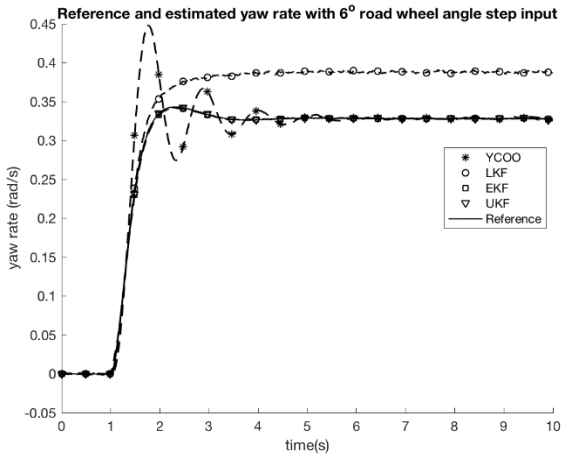

Figure 19 - Yaw rate estimation using different strategies with 6° road wheel angle step input.

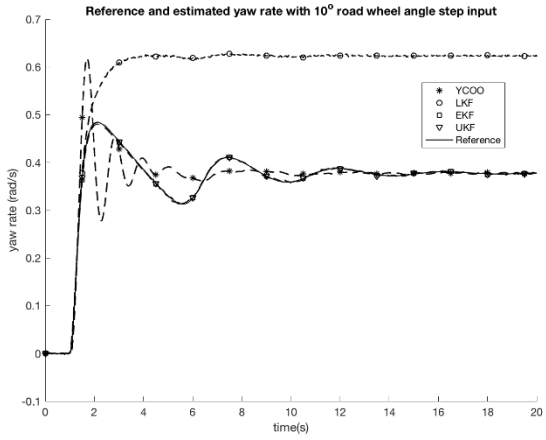

Figure 20 - Yaw rate estimation using different strategies with 10° road wheel angle step input.

3.3 Robustness Test

3.3.1 Vehicle Mass variation

Figure 21 shows the yaw rate estimation with different strategies with a 30% increase in the vehicle mass and a 2º road wheel angle step input. It illustrates that all Kalman filter types are sensitive to the vehicle mass variation and do not have good robustness characteristics with respect to this parameter. These results suggests that if the Kalman Filters are tuned to have good sensor noise rejection capabilities, meaning more confidence is given to the model, and if the sensitivity of the filters are high with respect to the model parameter changes, then this will negatively impact the estimation performance. However, it is interesting to observe that the YCOO performance has not been impacted with respect to this parameter variation. It could be argued that the plant parameter variations occur in the low frequency region where the YCOO is designed to have a closed loop sensitivity transfer function with a small magnitude resulting in a good robustness characteristic.

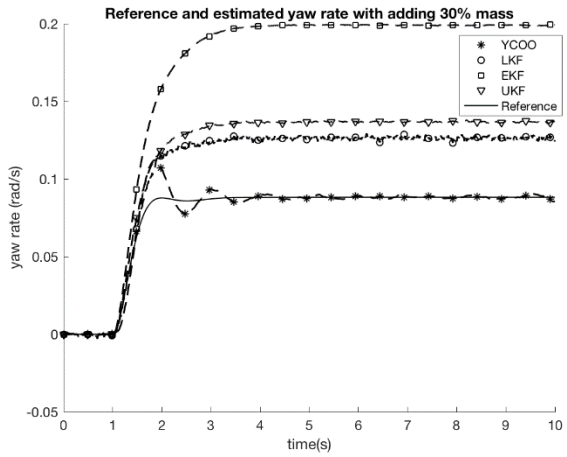

Figure 21 - Yaw rate estimation using different strategies with +30% mass.

3.3.2 Tire-road coefficient of friction

The yaw rate estimation results with a reduced tire-road coefficient of friction $\mu = 0.5$ (this coefficient for dry asphalt is equal to $0.9 - 1$) and a 2^o road wheel angle step input are shown in Figure 22. The results indicate that all strategies are not very sensitive to the changes in μ as they are to the vehicle mass variations. Comparatively, EKF is more sensitive to μ than the other strategies.

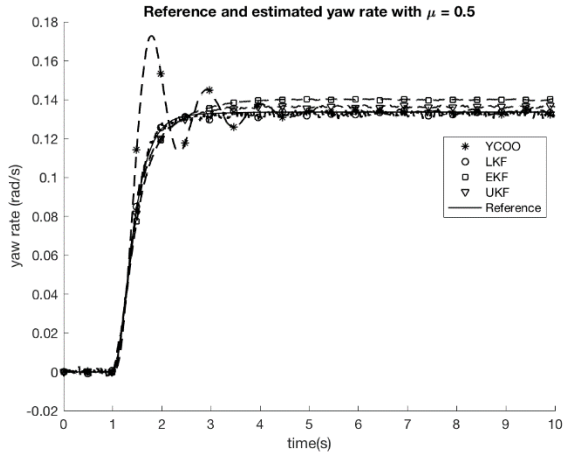

Figure 22 - Yaw rate estimation using different strategies with μ=0.5.

4 State Estimation, The MIMO Case

In the MIMO case, we increase the number of vehicle model inputs to two -- by adding rear road wheel angle and making the vehicle model four-wheel steering. By addition of one more input to the system, we expect a positive impact on both the performance and robustness of these

estimators. The vehicle model includes two inputs: the front and rear road wheel angles (δ_f, δ_r), and two outputs: the front and rear axle lateral accelerations (a_f, a_r). The model states are the vehicle sideslip angle β and yaw rate ω, as shown in Figure 5.

4.1 Youla Parameterization Control Design

Given the state space representation of the vehicle model, with known matrices A_e, B_e, C_e and D_e, we can derive the transfer function matrix of the plant using the following,

$$G_{p,e} = C_e(sI - A)^{-1}B_e + D_e \tag{37}$$

Based on the YCOO MIMO control and estimation design in [1], with the resulting transfer function matrix $G_{p,e}$, we derive the Smith-McMillan form of this TFM (transfer function matrix).

First, the plant TFM is written in the factorized form,

$$G_p = N_r D_r^{-1} = \begin{pmatrix} N_{11} & N_{12} \\ N_{21} & N_{22} \end{pmatrix} \begin{pmatrix} DEN & 0 \\ 0 & DEN \end{pmatrix}^{-1} \tag{38}$$

N_r is the numerator polynomial matrix and D_r is the decoupled denominator. Then, we utilize the standard approach for deriving the Smith-McMillan form of this TFM using the greatest common divisor (GCD) of all $K \times K$ minors, where $D_0 = 1$, and $D_K = GCD$ of all $K \times K$ minors. Using this approach, we can write,

$$D_1 = 1, \qquad D_2 = \det N_r$$

$$G_p^{SM} = \begin{pmatrix} \frac{D_1}{D_0} & 0 \\ 0 & \frac{D_2}{D_1} \end{pmatrix} \begin{pmatrix} \frac{1}{DEN} & 0 \\ 0 & \frac{1}{DEN} \end{pmatrix} = N_{SM} D_{SM}^{-1} \tag{39}$$

where D_0, D_1, and D_2 are the greatest common divisors of the polynomial matrix N_r, $N_{SM} = \begin{pmatrix} 1 & 0 \\ 0 & D_2 \end{pmatrix}$, and $D_{SM} = D_r$.

Given the following relationship between G_p^{SM} and G_p,

$$G_p(s) = u_L^{-1} G_p^{SM} u_R^{-1} \tag{40}$$

then, it can be shown that the unimodular matrices u_L and u_R can be computed by

$$u_L = (N_r N_{SM}^{-1})^{-1} \tag{41}$$

$$u_R = D_r D_{SM}^{-1} \tag{42}$$

The S-M form or the decoupled plant TFM has the following form,

$$G_p^{SM}(s) = \begin{pmatrix} G_{p1} & 0 \\ 0 & G_{p2} \end{pmatrix} = \begin{pmatrix} \frac{1}{(s+p_1)(s+p_2)} & 0 \\ 0 & gs^2 \end{pmatrix} \quad (43)$$

where g is a gain and the plant has two LHP poles and two zeros at the origin. The Youla transfer functions designed for the decoupled plant have the following structures,

$$Y_1 = \frac{1}{G_{p1}} \frac{\omega_n^2}{(s^2 + 2\zeta\omega_n s + \omega_n^2)(\tau s + 1)} \quad (44)$$

$$Y_2 = \frac{K}{(s^2 + 2\zeta\omega_n s + \omega_n^2)(\tau_1 s + 1)^2(\tau_2 s + 1)^2} \quad (45)$$

where the gain K is selected to be,

$$K = \frac{\tau^2 + 2\zeta\omega_n\tau_2 + \omega_n^2}{g\tau_2^2} \quad (46)$$

The gain K is selected so that the closed loop transfer function, T_2, associated with Y_2, is at 0db in the low frequency region for good target or reference following. The extra poles at $s = 1/\tau_1$ in Y_1 and Y_2 transfer functions are included to reduce their gains at high frequency. The extra poles at $s = 1/\tau_2$ in Y_2 are for canceling the effect of zeros of G_p^{SM} at the origin so that the closed loop TFM target following at low frequency is not drastically compromised as discussed in detail below. The coupled Youla TFM can be computed from the decoupled Youla TFM using the previously calculated unimodular matrices,

$$Y = u_R M_y u_L \quad (47)$$

where

$$M_y = \begin{pmatrix} Y_1 & 0 \\ 0 & Y_2 \end{pmatrix} \quad (48)$$

Then we can derive the close-loop transfer function matrix T_y and sensitivity transfer function matrix S_y from the decoupled system using the following relationships,

$$T_y(s) = u_L^{-1} G_p^{SM} M_y u_L \quad (49)$$

$$S_y(s) = u_L^{-1}\left(I - G_p^{SM} M_y\right) u_L \quad (50)$$

Then the transfer function matrix of the resulting controller, G_c, can be computed by

$$G_c(s) = u_R\left(I - M_y G_p^{SM}\right) u_L \quad (51)$$

The plot of singular values for T_y, S_y, and Y are shown in Figure 23. Both maximum and minimum values of T_y are at 0db in the desired frequency region, which enforces a good target following for the closed loop system. Since the second decoupled plant transfer function, G_{p2}, includes two zeros at the origin, we need to modify the closed-loop transfer function by adding two poles at $s = 1/\tau_2$ so that the closed loop transfer function behaves as a bandpass filter for ensuring its target following capability at the low frequency is not significantly compromised, as

shown in Figure 23. The singular values of Y are low at high frequency which results in good sensor noise attenuation at the plant input.

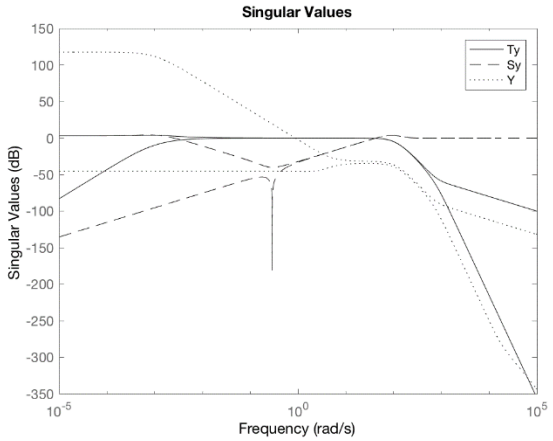

Figure 23 - Singular values of Ty, Sy, and Y.

4.2 Simulation and Estimation Result

The yaw rate estimations for 2^o road wheel angle step inputs are shown in Figure 24. With an additional input, the rear road wheel angle, the YCOO's transient response performance is significantly improved. The response of YCOO is very similar to both the EKF and UKF. The LKF still has a small steady state error due to the small difference between the linear model used for estimation and the nonlinear vehicle and tire models of the reference generator. The vehicle sideslip estimations for 2^o road wheel angle step inputs are shown in Figure 25. Except for the LKF, all other strategies have excellent transient and steady state responses.

The yaw rate estimation for the wheel angle step inputs of 4^o are illustrated in Figure 26. The steady state error of LKF has clearly increased as the difference between the linear estimation model and the reference generator model is becoming more significant. Again the YCOO, EKF, and UKF have excellent transient and steady state responses. The excellent performance of the YCOO, in this case, is unexpected as YCOO, similar to LKF, uses a linear model for the state estimation.

The vehicle sideslip estimation for 4^o road wheel angle step inputs are shown in Figure 27. In this case, it seems that the steady state error of the LKF has reduced when compared to the smaller wheel angle input results. However, this is misleading: Depending on vehicle geometry and the way the front and rear wheel steering angles are controlled, the vehicle can obtain a large yaw rate without a large slip angle. So, the large steady-state error in the yaw rate estimation (as is the case with the LKF), could result in a reduced steady state error in the vehicle sideslip estimation when the tire lateral forces are close to saturation. All other strategies again have excellent performances in both transient and steady state responses.

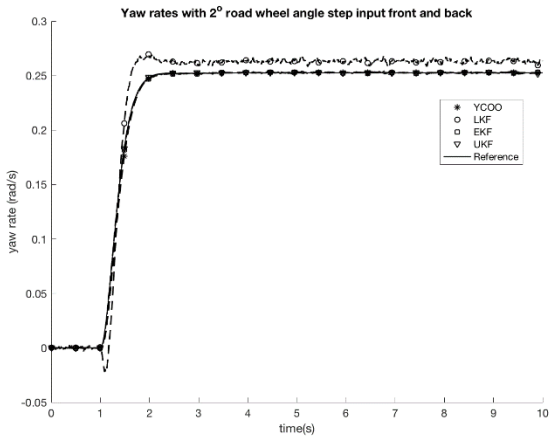

Figure 24 - The yaw rate estimation results for different strategies, MIMO case.

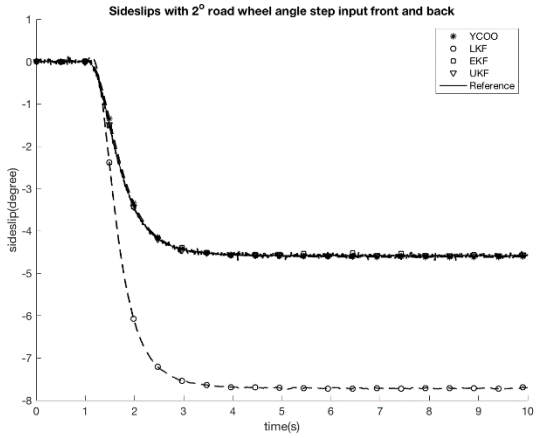

Figure 25 - The vehicle sideslip estimation for different strategies, MIMO case.

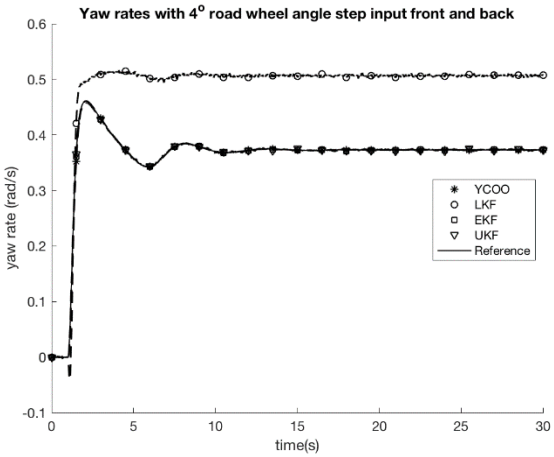

Figure 26 - The yaw rate estimation results for different strategies with 4o road wheel angle step input, MIMO case.

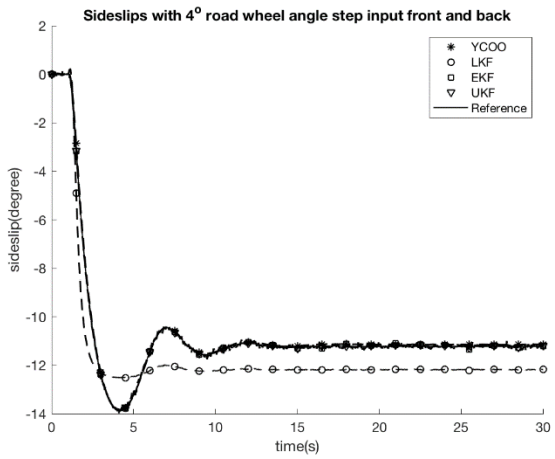

Figure 27 - The vehicle sideslip estimation results for different strategies with 4o road wheel angle step input, MIMO case.

4.3 Robustness Test

4.3.1 Vehicle mass variation

The yaw rate and vehicle sideslip estimation results with a 30% increase of mass are shown in Figure 28 and Figure 29. All Kalman filtering types do not have good robustness with respect to the vehicle mass variation, the results in this case are similar to the SISO case. However, the YCOO has excellent robustness characteristics with respect to the vehicle mass variation.

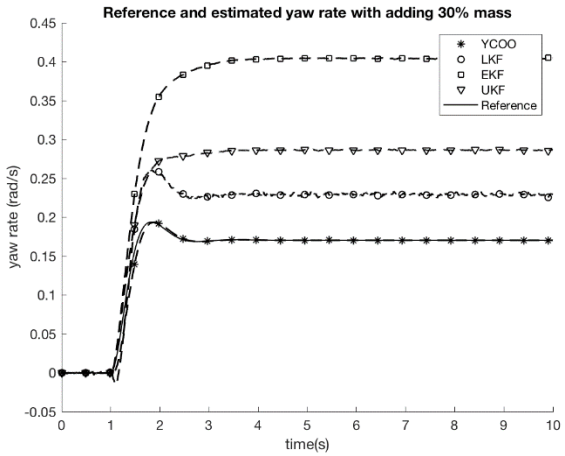

Figure 28 - The yaw rate estimations for different strategies with 30% additional mass, MIMO case.

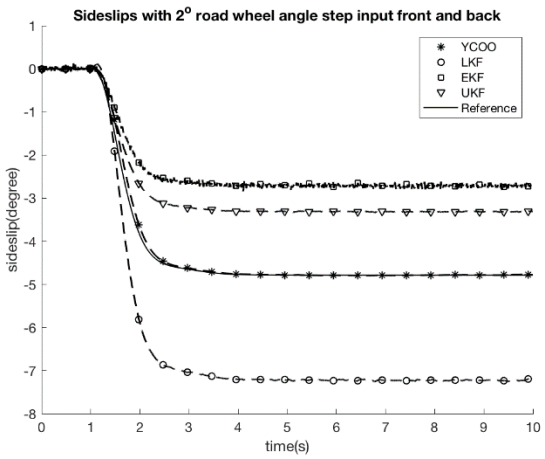

Figure 29 - The vehicle sideslip estimations for different strategies with 30% additional mass, MIMO case.

4.3.2 Tire-road coefficient of friction

The yaw rate estimations for the reduced tire-road coefficient of friction, $\mu = 0.5$, are shown in Figure 30. Unlike the SISO case, by the addition of rear wheel steering to the vehicle model, all Kalman filtering strategies have become more sensitive to the scaling of lateral tire forces. However, the YCOO has capitalized on this second input, based on its MIMO estimation design strategy, to drastically improve both its transient and steady state responses with respect to the changes of this parameter. For the Vehicle sideslip estimation results of Figure 31, similar argument as for the yaw rate estimations apply.

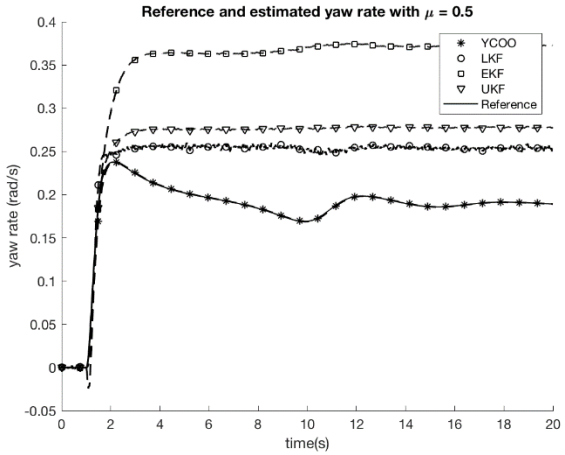

Figure 30 - The yaw rate estimations for different strategies with μ=0.5, MIMO case.

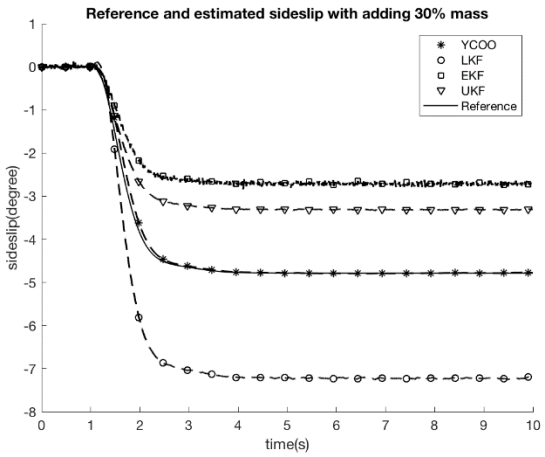

Figure 31 - The vehicle sideslip estimations for different strategies with μ=0.5, MIMO case.

4.4 Sensor Bias

Besides the sensor noise, the sensor bias is another source of uncertainties as sensor measurements normally include an offset. This offset includes the calibration error and drift over lifetime due to temperature and supply voltage variations. The sensor bias of the accelerometer type proposed in this study is within the range of $\pm 1\ m/s^2$ [7]. If we assume both the front and rear accelerometers have the same value for sensor bias, then in the case of YCOO, the yaw rate estimation is not affected by this offset as illustrated in Figure 32.

Although we are using a dynamic model in YCOO, the observation and feedthrough matrices (C_e and D_e) are derived from the kinematic relationship between lateral accelerations and states. Therefore, as YCOO estimates the yaw rate, the sensor bias of the front and rear accelerometers are canceled out. But the story is different for the case of vehicle sideslip estimation, in this case, the bias has a large influence on the estimation result.

Since the YCOO tries to track the reference generator output signal (measured signal), the error due to the sensor bias will accumulate over time and estimation will have a significant offset with respect to the reference/measured signal as shown in Figure 33. In the case of Kalman filters, the LKF has relatively large steady state error due to the sensor bias. However, the EKF and especially the UKF, due to its statistical sampling technique for selecting appropriate sample points, are not relatively affected by the sensor bias.

We have designed a sensor bias estimation strategy to eliminate the negative impact of the sensor bias on the YCOO estimation strategy, as illustrated in Figure 34. The sensor bias estimation strategy is a subject of a current invention disclosure.

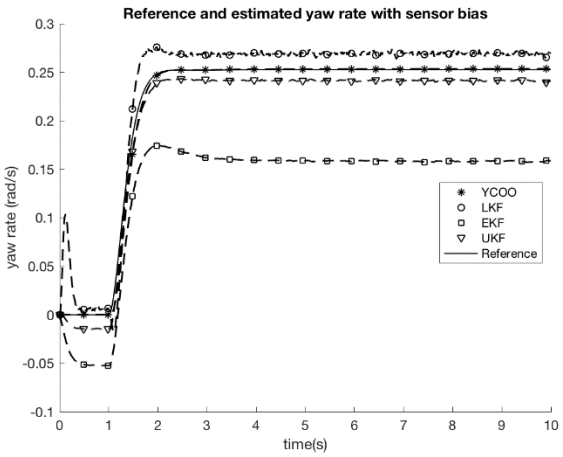

Figure 32 - The yaw rate estimation of different strategies with a sensor bias of 1 m/s^2.

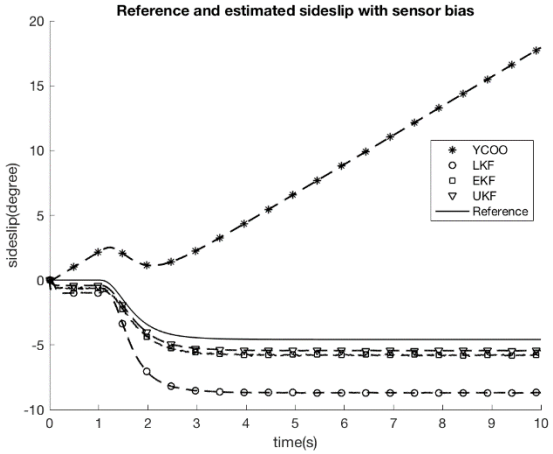

Figure 33 - The vehicle sideslip estimations for different strategies with a sensor bias of 1 m/s^2.

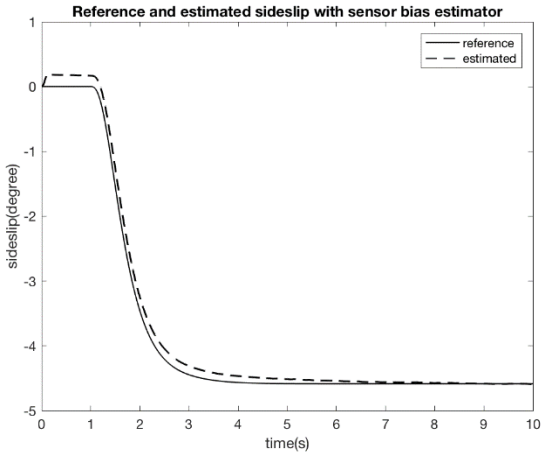

Figure 34 - The vehicle sideslip estimation of YCOO including sensor bias estimator.

5 Conclusion and Future Work

We investigated the performance and robustness of various estimation concepts using a common application. A front wheel steering vehicle model with the measurement of its lateral acceleration at the c.g. along with four-wheel steering with two lateral acceleration measurements at the front and rear axles are used for this application. Various road wheel angle step input sizes are used to illustrate the performance and robustness of these estimators. The new YCOO SISO and MIMO estimation technique showed excellent potential when compared to Kalman filtering techniques such as LKF, EKF, and UKF.

Kalman Filters did not show relatively strong results in the robustness tests in this application. However, one can imagine using adaptive Kalman Filtering techniques to increase their robustness characteristics when facing parameter variations such as vehicle mass and tire-road coefficient of friction. Although, the MIMO YCOO does illustrate excellent robustness results when varying vehicle mass and tire-road coefficient of friction, it turns out that it is sensitive to the longitudinal speed variations, which is assumed constant in all the presented simulations. Therefore, it is also possible to modify the YCOO, for example by using Linear Parameter Varying (LPV) techniques, or AI strategies such as Q-learning to reduce its sensitivity to all parameter variations including the longitudinal speed.

It is in our future plan to address the topics mentioned above. In addition, we are planning to analytically shed more light onto the robustness properties of these estimation techniques by deriving the appropriate sensitivity functions with respect to the various parameters mentioned in this application. Finally, our plan is to test these estimation concepts either on a real vehicle or verify the results with a more sophisticated vehicle model, such as CarSim.

References

[1] F. Assadian, A. K. Beckerman and J. Velazques Alcantar, "Estimation Design Using Youla Parametrization With Automotive Applications," *Journal of Dynamic Systems, Measurement, and Control,* vol. 140, no. 8, 2018.

[2] R. E. Kalman, "A new approach to linear filtering and prediction problems.," *Transactions of the ASME - Journal of Basic Engineering,* vol. 82, no. D, pp. 35-45, 1960.

[3] Y. Wang, R. Rajamani and A. Zemouche, "Sequential LMI approach for the design of a BMI-based robust observer state feedback controller with nonlinear uncertainties," *International journal of robust and nonlinear control,* vol. 28, no. 4, pp. 1246-1260, 2018.

[4] H. F. Grip, L. Imsland, T. A. Johansen, J. C. Kalkkuhl and A. Suissa, "Vehicle sideslip estimation," *IEEE control systems magazine,* vol. 29, no. 5, pp. 36-52, 2009.

[5] T. Fiorenzani, C. Manes, C. Oriolo and P. Peliti, "Comparative study of unscented kalman filter and extended kalman filter for position/attitude estimation in unmanned aerial vehicles," Institute for Systems Analysis and Computer Science (IASI-CNR), Rome, 2008.

[6] H. Pacejka, Tire and vehicle dynamics, Elsevier, 2005.

[7] A. T. Van Zanten, "Bosch ESP systems: 5 years of experience," *SAE Technical Paper*, Vols. No. 2000-01-1633, 2000.

[8] JVa, "SCA830-D05 Single Axis Accelerometer with Digital SPI Interface," VTI Technologies Oy, 2019. [Online]. Available: https://www.murata.com/~/media/webrenewal/products/sensor/accel/auto_digital/sca830-d05_accelerometer_0.ashx?la=zh-cn. [Accessed 1 11 2019].

Appendix: Kalman Filter Algorithms

A.1 Kalman Filter

Suppose we have a discrete state space system with additive noises w_d and v_d

$$x(k+1) = A_d x(k) + B_d u(k) + w_d(k) \tag{52}$$

$$y(k) = C_d x(k) + D_d u(k) + v_d(k) \tag{53}$$

where $x(k)$ is the state after k steps at $t = k\,\mathrm{d}t$. $u(k)$ is a known input, and $y(k)$ is the measurement of the output at $t = k\,\mathrm{d}t$.

$w_d(k)$ and $w_d(k)$ are process noise and sensor noise respectively, and they are of Normal Distribution of with the same means, $\mu = 0$ but different variances, $\sigma^2 = Q_d$ and $\sigma^2 = R_d$ respectively.

If we have a state space representation in continuous time domain, we can discretize it before designing a Kalman filter. For a continuous-time state space system,

$$\dot{x}(t) = Ax(t) + Bu(t) \tag{54}$$

$$y(t) = Cx(t) + Du(t) \tag{55}$$

We can discretize it using the following equations

$$A_d = e^{A\mathrm{d}t} \tag{56}$$

$$B_d = \int_0^{\mathrm{d}t} e^{Av}\, B\mathrm{d}v = A^{-1}\left(e^{a\mathrm{d}t} - I\right)B \tag{57}$$

$$C_d = C, \qquad D_d = D \tag{58}$$

For designing the Kalman filter, there are two stages: prediction stage, and innovation stage. With initial condition $x(0) = x_0$, $P(0) = P_0$ where x_0 is the initial states value and P_0 is the initial covariance, at prediction stage:

$$\hat{x}(k+1) = A_d x(k) + B_d u(k) \tag{59}$$

$$\hat{P}(k+1) = A_d P(k) A_d^T + Q_d \tag{60}$$

Next we need to adjust the Kalman Gain to obtain the balance between model estimation and sensor measurement.

$$K_f(k+1) = \hat{P}(k+1) C_d^T \left[C_d \hat{P}(k+1) C_d^T + R_d\right]^{-1} \tag{61}$$

Using this Kalman Gain, we can correct our states by the measurement.

$$x(k+1) = \hat{x}(k+1) + K_f(k+1)[y(k+1) - C_d \hat{x}(k+1) - Du(k+1) \tag{62}$$

$$\hat{P}(k+1) = \left[I_n - K_f(k+1) C_d\right] \hat{P}(k+1) \tag{63}$$

A.2 Extended Kalman Filter

We have a continuous time nonlinear system

$$\dot{x}(t) = f\big(x(t), u(t)\big) + w(t) \tag{64}$$

$$y(t) = h\big(x(t), u(t)\big) + v(t) \tag{65}$$

where $w(t)$ is process noise and $v(t)$ is sensor noise.

$$w \sim N(0, Q) \tag{66}$$

$$v \sim N(0, R) \tag{67}$$

Then we can calculate the derivative of the state \dotx and the variance matrix \dotP directly

$$K(t) = P(t) H^T(t) R^{-1} \tag{68}$$

$$\dot{x}(t) = f\big(x(t), u(t)\big) + K(t)\big[y(t) - h\big(x(t)\big)\big] \tag{69}$$

$$\dot{P}(t) = F(t)P(t) + P(t)F^T(t) - K(t)H(t)P(t) + Q \tag{70}$$

where

$$F_{ij}(t) = \frac{\partial f_i}{\partial x_j} \tag{71}$$

$$H_{ij}(t) = \frac{\partial h_i}{\partial x_j} \tag{72}$$

$$F(t) = \big\{F_{ij}(t)\big\};\ \ H(t) = \big\{H_{ij}(t)\big\} \tag{73}$$

But having an extended Kalman filter in continuous domain may not be very practical. So we need to implement the continuous system into the discrete time extended Kalman filter. Recall we have a continuous time nonlinear system

$$\dot{x}(t) = f\big(x(t), u(t)\big) + w(t) \tag{74}$$

$$y(t) = h\big(x(t), u(t)\big) + v(t) \tag{75}$$

we can linearize the equations at each time step, and the resulting discrete time equations are

$$\mathrm{d}x_k = f(x_k, u_k)\mathrm{d}t \tag{76}$$

$$x_{k+1} = x_k + \mathrm{d}x_k = x_k + f(x_k, u_k)\mathrm{d}t = f_k(x_k, u_k) \tag{77}$$

$$y_k = h_k(x_k, u_k) \tag{78}$$

and the algorithm of extended Kalman Filter is

$$\hat{x}_k = f_k(x_{k-1}, u_{k-1}) \tag{79}$$

$$\hat{P}_k = A_{k-1}P_{k-1}A_{k-1}^T + Q \tag{80}$$

$$L_k = \hat{P}_k H_k^T \big(H_k \hat{P}_k H_k^T + R\big)^{-1} \tag{81}$$

$$x_k = \hat{x} + L_k\big(y_k - h_k(\hat{x}, u_k)\big) \tag{82}$$

$$P_k = \hat{P}_k - L_k H_k \hat{P}_k \tag{83}$$

where$A_k = e^{F(t)\mathrm{d}t}$, $H_k = H(t)$, where $t = kdt$ and $F(t)$ and $H(t)$ are values obtained from Equations (71) and (72).

A.3 Unscented Kalman Filter

We have a continuous time nonlinear system with additive noise

$$\dot{x}(t) = f\big(x(t), u(t)\big) + w(t)$$

$$y(t) = h\big(x(t), u(t)\big) + v(t)$$

where w(t) is process noise and v(t) is sensor noise.

$$w \sim N(0, Q)$$

$$v \sim N(0, R)$$

To discretize the continuous system, we can use Equations (76) to (78) or other numerical method to evaluate the value at each time step. For unscented Kalman filter using $2n$ sigma points, the algorithm of unscented Kalman filter is:

First select $2n$ sigma points. Then, the i-th sample point at time step k is defined as follows

$$\hat{x}^{(i)}_{k-1|k-1} = \hat{x}_{k-1} + \left(\sqrt{nP_{k-1}}\right)^T_i, \qquad i = 1, 2, 3, \dots, n \tag{88}$$

$$\hat{x}^{(n+i)}_{k-1|k-1} = \hat{x}_{k-1} - \left(\sqrt{nP_{k-1}}\right)^T_i, \qquad i = 1, 2, 3, \dots, n \tag{89}$$

Propagate each sigma point through the state equation

$$\hat{x}^{(i)}_{k|k-1} = f_k\left(\hat{x}^{(i)}_{k-1|k-1}, u_{k-1}\right), \qquad i = 1, 2, 3, \dots, n$$

$$\hat{y}^{(i)}_{k|k-1} = h_k\left(\hat{x}^{(i)}_{k-1|k-1}, u_{k-1}\right), \qquad i = 1, 2, 3, \dots, n$$

Calculate the mean and variance of the sigma points

$$\hat{x}_{k|k-1} = \frac{1}{2n}\sum_i^{2n} \hat{x}^{(i)}_{k|k-1} \tag{92}$$

$$P_{k|k-1} = \frac{1}{2n}\sum_i^{2n}\left(\hat{x}^{(i)}_{k|k-1} - \hat{x}_{k|k-1}\right)\left(\hat{x}^{(i)}_{k|k-1} - \hat{x}_{k|k-1}\right)^T + Q \tag{93}$$

$$\hat{y}_{k|k-1} = \frac{1}{2n}\sum_i^{2n} \hat{y}^{(i)}_{k|k-1} \tag{94}$$

$$P_{xy} = \frac{1}{2n}\sum_{i}^{2n}\left(\hat{x}_{k|k-1}^{(i)} - \hat{x}_{k|k-1}\right)\left(\hat{y}_{k|k-1}^{(i)} - \hat{y}_{k|k-1}\right)^{T} \quad (95)$$

$$P_{y} = \frac{1}{2n}\sum_{i}^{2n}\left(\hat{y}_{k|k-1}^{(i)} - \hat{x}_{k|k-1}\right)\left(\hat{y}_{k|k-1}^{(i)} - \hat{x}_{k|k-1}\right)^{T} + R \quad (96)$$

Update the state with calculated variance and covariance

$$\hat{x}_{k|k} = \hat{x}_{k|k-1} + P_{xy}P_{y}^{-1}\left(y_{k} - \hat{y}_{k|k-1}\right) \quad (97)$$

$$P_{k|k} = P_{k|k-1} - P_{xy}P_{y}^{-1}P_{xy}^{T} \quad (98)$$